Interface effects on the fracture mechanism of a high toughness aluminum composite laminate

C.M. Cepeda-Jiménez[a]*, M. Pozuelo[b], J.M. García-Infanta[a], O.A. Ruano[a], F. Carreño[a]

[a]*Departamento de Metalurgia Física, CENIM, CSIC, Av. Gregorio del Amo 8, 28040 Madrid, Spain*

[b]*Department of Materials Science and Engineering, 6531-G Boelter Hall, University of California, Los Angeles, CA 90095-1595, USA*

Abstract

The microstructure and the mechanical properties of a multilayer composite laminate based on aluminum 7075 and 2024 alloys produced by hot roll-bonding were examined. The composite laminate has been tested at room temperature under impact Charpy tests, three-point bend tests and shear tests on the interfaces. The toughness of the post-rolling tempered and T6 treated composite laminate, measured by impact absorbed energy in the crack arrester orientation, was more than twenty times higher than that of the monolithic Al 7075 alloy and seven times higher than that of Al 2024 alloy. The outstanding toughness increase of the composite laminate in the post-rolling tempered and T6 treated condition is mainly due to the mechanism of "interface pre-delamination". By this fracture mechanism the interfaces are debonded before the main crack reaches them, warranting delamination in all interfaces. Therefore, delamination and crack renucleation in every layer are responsible for the improvement in toughness.

Keywords: Multilayer aluminum composite laminates; Impact toughness; Delamination; Fracture mechanism; Hot roll-bonding

*Corresponding author. Tel.: +34 91 5538900; fax: +34 91 5347425.

E-mail address: cm.cepeda@cenim.csic.es (C.M. Cepeda-Jiménez)

1. Introduction

The aluminum industry has a long record of improving the performance of aerospace alloys. This has resulted in the development and progressive application in commercial aircraft of very high strength 7xxx alloys and high damage tolerance 2xxx and 6xxx alloys [1-3]. However, the big challenge still is to achieve high strength-good damage tolerance alloys for thick section applications. Although the aluminum industry continues to develop higher performance alloys, an additional and complementary avenue for improving the performance of airframes structures is becoming increasingly interesting: optimizing the utilization of materials. In this sense, it could be possible to improve the damage tolerance of metallic structures by

modifying conventional design configurations to take maximum profit from the strong points of aluminum alloys and de-emphasize their weaker points [4-6].

Laminated metal composites (LMCs) consist of alternating metal or reinforced metal layers that are bonded with "sharp" interfaces. LMCs can dramatically improve many properties including toughness, fatigue behavior, impact behavior, wear, corrosion, and damping capacity; or provide enhanced formability or ductility [7-14]. From a mechanical viewpoint, optimizing the combination of strength, toughness and interface bonding is the basis for lamination. The toughness and impact behavior in many respects are the most interesting issues from the viewpoint of their applicability.

Hot rolling is capable of obtaining good bonds between layers, while refining the microstructure, improving toughness [15,16]. The interfaces that may delaminate are responsible for the high impact and fracture resistance of the multilayer materials and contribute to increase the extrinsic toughening by different mechanisms. Delamination in the layers ahead of the crack tip results in a reduction and redistribution of the local stress [17,18]. In the case of ultrahigh carbon steel (UHCS) based composite laminates, it has been shown that interlayer delamination is the principal mechanism of crack arresting [19,20]. This process makes crack propagation through the composite very difficult.

The main objective in this research is to study the influence of processing and thermal treatments on the microstructure and interfacial mechanical properties of an aluminum multilayer material with high specific strength and outstanding toughness. The second objective is the study of extrinsic mechanisms responsible of the toughness increase in the processed composite. For this purpose, a composite laminate that consists of 11 alternate layers of 7075 aluminum alloy and 2024 aluminum alloy was processed by hot roll-bonding.

2. Experimental procedure

2.1. Materials and processing

The aluminum alloys used in the present study were rolled sheets, 2 mm in thickness, of Al-Zn 7075-T6 alloy (termed "D") and Al-Cu 2024-T3 (termed "L").

The 7075-T6 is the strongest and most widely used form of this alloy. On the other hand, one of the most important properties of 2024 aluminum alloy is that the solid solution treatment is not as critical as that of 7075 aluminum alloy. This alloy can be aged naturally (T3 temper) or artificially (T6 temper) [21]. The composition in atomic percentage of the alloys is included in **Table 1** and some mechanical properties are summarized in **Table 2**. The as-received aluminum alloy sheets were cleaned with acetone. Then, six 7075 aluminum layers and five 2024 aluminum layers of dimensions 60 mm in width and 150 mm in length were stacked alternately, making up a bundle 22 mm thick and referenced in this work as ADL11.

The stacked aluminum material was welded by Tungsten Inert Gas (TIG) at their edges to avoid oxygen penetration and delamination during processing, and then hot-rolled at 465 ºC in several passes without lubrication. After rolling, the welding edge was completely removed.

The processing temperature was selected to be the solution temperature for the 7075 aluminum alloy (D). The diameter of the rolls was 130 mm and the rolling speed was 334 mm/s. All rolling directions were parallel to the rolling direction of the as-received sheets. Without changing the rolling direction, the rolling process was repeated up to five cycles of several passes of about 4-8% reduction per pass, with the sample being reheated at 465ºC between series. **Figure 1** shows the processing scheme followed on the composite laminate, accumulating a total reduction in thickness of 2.3:1, corresponding to an equivalent strain of ε=0.95 (according to Von Misses criterion).

The resulting hot-rolled sample was in the form of a plate, of thickness about 10 mm, length about 350 mm and width about 60 mm. The average thickness of the aluminum layers in the ADL11 laminate was ~920 μm.

After hot rolling, and due to the high temperatures employed during the processing, it was necessary to carry out a heat treatment to improve the mechanical properties of the aluminum alloys included in the composite laminate. The heat treatment that has been deemed optimal for the 7075 alloy is the T6 treatment. This heat treatment involves solution treatment at 465 ºC for 30 min, followed by rapid quenching in water and finally age hardening at 135 ºC for 14 h.

Several samples of as-rolled composite laminate were subjected to a post-rolling tempering at 175ºC during 6h [22] before the T6 heat treatment, in order to allow recovery of the deformed microstructure and to avoid the premature failure of the interfaces.

2.2. Microstructural determination

Microstructure at the bond interfaces in the L-T orientation was observed by scanning electron microscopy (SEM) using a JEOL JSM 6500F equipment with field emission gun. The chemical composition of laminate interfaces was examined by an electron probe microanalyzer (Oxford Inca) operating at 15 kV. Metallographic observation involved methods of standard surface preparation. The samples were electropolished in a 30% nitric acid solution in methanol at -15 ºC and 15 V. This is the most favorable condition for the higher strength 7075 aluminum alloy.

2.3. Mechanical tests

2.3.1. Microhardness test

Microhardness measurements were conducted at the region close to the laminate interfaces with a Vickers indenter under loads of 100 g for 15 s.

2.3.2. Three point bend test

Three point bend tests were carried out using two mm V-notched Charpy type specimens (10x10x55 mm^3) in the crack-arrester orientation being the loading span 40 mm. In crack arrester orientation the crack is forced to pass through each layer sequentially. This configuration is the most interesting, both technically and scientifically, to study the different fracture mechanisms operating during the bend test. Then, load vs. displacement was recorded in order to characterize the mechanical response to layer fracture and crack propagation across the laminate.

The bending was performed using a *Servosis* universal test machine under displacement control at a rate of 0.04 mm/s, with load and time recorded by the data acquisition program. At least two samples for each thermal treatment considered were used to collect data. Fracture surface of selected specimens were examined by both macroscopic observations and optical microscopy to evaluate deformation micromechanisms and any interlayer debonding.

2.3.3. Shear test

The bonding of aluminum surfaces is a crucial step in the present process. The interface mechanical properties were measured by shear test in a *Servosis* universal test machine (cross-head rate=0.005 mm/s) using specimens of approximate dimensions 10x10x3 mm^3. The test was performed by clamping the sample between two metal supports (**Figure 2**). The interface to be tested is located just outside the border of the tool and parallel to the load direction. Then, a square punch at a given gap distance is used to apply the shear load until failure of the interface. The shear stress, τ, and the shear strain, γ, are given by the expressions [23]:

$$\tau = p/ae \qquad \gamma = \tan(\alpha) = d/l_{gap} \qquad (2)$$

where a is the initial width of the sample, e the initial thickness, p the force applied on the sample, d the midspan displacement, α is the shear angle and l_{gap} is the distance between the supports and the mobile punch, corresponding to 0.35 mm in this study.

2.3.4. Charpy test

Two mm V-notched Charpy type testing specimens were machined to 10x10x55 mm^3 dimensions from as-received monolithic Al 7075 (D) and Al 2024 (L) aluminum alloys, and ADL11 composite laminate. For the as-received materials Charpy samples were machined from rolled plates of 12 mm in thickness. The samples were tested both in the crack arrester and divider orientation. For the monolithic materials, in the crack arrester orientation the notch tip is parallel to the rolling plane and rolling direction. Accordingly, in the crack divider orientation the notch tip is perpendicular to the rolling plane and rolling direction. The crack arrester orientation for the composite laminate was defined previously. In the crack divider orientation, the initial notch/crack tip intersects all the layers of the test sample and therefore the crack front encounters all the layer interfaces simultaneously. Charpy impact testing was conducted on a pendulum impact tester with a maximum capacity of 294 J. Three samples for the as-received alloys and the post-rolling tempered and T6 treated composite laminate were tested.

3. Results

3.1. Microstructure

The microstructure of the as-received Al 7075 rolled sheet in the "LT" orientation is presented in **Figure 3a**. The as-received material shows large grains (10-20 μm) that are elongated and flattened parallel to the rolling direction. The insoluble iron-rich intermetallic particles and partially soluble constituent particles were observed to be randomly distributed in the as-received sheet. These intermetallic particles ranged in size from approximately 0.5 to 5 μm. The equilibrium precipitate $MgZn_2$, which is the main strengthening particle [24], was not observed in the SEM micrograph due to its small size.

The microstructure of the as-received Al 2024 rolled sheet in the "LT" orientation is presented in **Figure 3b**. This microstructure consists of recrystallized grains that are less elongated than for the Al 7075. They have an average size of 10-20 μm and a relatively high fraction of second-phase precipitates (Al_2CuMg) located both at the grain boundaries and inside the grains. Several calorimetric studies about precipitation paths and kinetics in these alloys are reported in the literature [25] with some disagreements about the precipitation of intermediate phases subsequent to the GP zone formation. The Al-Cu-Mg alloys show two different aging paths depending on the Cu:Mg ratio. Two different stable phases can be present in a peak-aged sample according to the Al-Cu-Mg phase diagram [26]: θ ($CuAl_2$) and S (Al_2CuMg). According to Mondolfo [27] when Cu:Mg > 2 and Mg:Si > 1.7 (this case), the compound Al_2CuMg is formed. It is worth noting that for Mg:Si ratio approximately 1.7 then Mg_2Si and $CuAl_2$ are in equilibrium. In addition, for the Mg:Si ratio 1 or less, $Cu_2Mg_8Si_6Al_5$ is formed usually together with $CuAl_2$. On the other hand, the large precipitates in **Fig. 3b** are aluminides containing copper, iron and manganese, $(CuFeMn)Al_6$,or aluminides containing silicon, $(CuFeMn)_3Si_2Al_{15}$, in percentages much higher than in the metal matrix. The large size of this precipitates indicate that they were not affected by solution and aging treatment.

Figure 4 shows the microstructure of the third interface in the ADL11 composite laminate with (**4a** and **4b**) and without (**4c** and **4d**) post-rolling tempering at 175ºC for 6h previously to the T6 treatment. **Fig. 4a** and **c** correspond to regions close to the interface and **4b** and **d** correspond to regions in the Al 7075 alloy distant from the interface. The micrographs suggest a good bond, although further assessment of the bond integrity requires quantitative mechanical testing. White and bright particles, identified as Al_2O_3 by microanalysis, are observed homogeneously and continuously distributed along the interface. During rolling, the aluminum matrix is able to deform plastically. In contrast, the alumina on the interface is brittle and its response to the stress is by fracturing. The aluminum occupying the opened spaces left by the fractured alumina and the diffusion of elements in these spaces is responsible of the bonding between clean metal surfaces. Additionally, small black spots are due to pickings by the electrolyte during the electropolishing.

On the other hand, the microstructure of the post-rolling tempered and T6 treated composite laminate consists of fine grains, about 3 μm in size, both close and far from the interface as it is shown in **Figure 4a** and **4b**. However, the microstructure of the ADL11 composite laminate without post-rolling tempering shows close to the interface, **Fig. 4c**, grains larger and poorly delineated with curved and irregularly shaped boundaries, which are typical of partially recrystallized alloys. Distant from the interface, **Fig. 4d**, the microstructure consists of equiaxed grains, about 2 to 3 μm in size, that are finer than those close to the interface.

Figure 5 shows the microanalysis of interfacial regions of the ADL11 composite laminate with and without post-rolling tempering given by filled and open symbols respectively. The interfaces are assigned numbers to indicate their location in the composite laminate (for example, i3 means interface three counting from the most external interface). **Figure 5a** and **b** shows concentration gradients in atomic percentage of Zn and Cu, respectively, that are

attributed to diffusion of elements due to the high temperature and pressure during processing. The microanalysis of Zn and Cu composition in different interfaces demonstrates that the same element diffusion is produced across outer and inner interfaces. The width of the region where significant element diffusion is present is about 60 μm for the Zn diffusion (**Figure 5a**) and between 20-30 μm for the Cu diffusion (**Figure 5b**). The extent of the Zn diffusion is not influenced by the post-rolling tempering; in contrast, the Cu diffusion is increased with the post-rolling tempering.

3.2. Mechanical tests

3.2.1. Microhardness test

Microhardness measurements were carried out across the composite laminate interfaces (**Figure 6**). The T6 composite laminate without post-rolling tempering shows lower microhardness values both for the 7075 aluminum alloy (171 HV) and 2024 alloy (116 HV) than the as-received material (**Table 2**). On the other hand, the hardness of the post-rolling tempered composite laminate reached a value of 195 HV in the 7075 aluminum alloy and 120 HV in the 2024 aluminum alloy far from the interface. Thus, the post-rolling tempered 7075 aluminum alloy after processing has higher microhardness than the as-received material (188 HV). In contrast, the microhardness for the 2024 aluminum alloy in both laminates is similar, and lower than the as-received material (138 HV), because the thermal treatment carried out after the processing was the optimum for the Al 7075 alloy but not for the 2024 Al. Furthermore, as observed in **Figure 6**, the hardness gradient around the interface is higher for the post-rolling tempered sample. This result is expected due to the combined contribution of solute effects and fine grain size in the post-rolling tempered sample.

3.2.2. Three point bend test

Figure 7 shows load-displacement curves obtained from three point bend test for the monolithic as-received alloys and for two roll-bonding composite laminates, in the crack arrester orientation, in two conditions: as-rolled and post-rolling tempered and T6 treated. Both monolithic Al 7075 alloy and Al 2024 alloy present high bending loads, 10 and 8 kN respectively, but low ductility.

On the other hand, the as-rolled composite laminate presents a lower strength (5.5 kN) due to the high temperatures of the processing. In contrast, the post-rolling tempered and T6 treated composite laminate possesses a maximum bending load of 9.53 kN, which is higher than the value predicted by the rule of mixtures (9.12 kN). Additionally, the ductility is outstanding.

It is worth noting that the curve corresponding to the T6 treated ADL11 composite laminate without previous post-rolling tempering is not included in the graph because this material showed high brittleness in the interfaces as will be shown later.

On the other hand, the bend curves for both samples given in **Fig. 7**, as-rolled and post-rolling tempered and T6 treated samples, show a similar pattern: a) several load drops due to cracking of the different layers until the crack is arrested at the various interfaces, and b) plateau regions that correspond to plastic deformation at the next aluminum layer until the following load drop occurs at the critical strain needed for crack renucleation. However, the curve shapes

clearly reveal differences between the two samples. The curve corresponding to the post-rolling tempered and T6 treated composite laminate shows a higher number of load drops (about eight) than those for the as-rolled ADL11 composite laminate that evidences larger flat zones and only three load drops. The successive load drops followed by flat zones indicate fracture and delamination of the different layers of the composite. Therefore, delamination makes difficult the crack propagation in the next layer which must deform plastically until a new dominant crack is nucleated.

Additionally, the curve corresponding to the post-rolling tempered and T6 treated composite laminate shows several small peaks in the plateau regions without important load drops, which may be associated with delamination in the next interface before the crack reaches it. This fracture mechanism, "interface pre-delamination" will be discussed later. These small load drops are not observed for the as-rolled composite laminate, indicating higher interface toughness in this laminate.

Figure 8 shows macrographs of ADL11 samples after bend testing: a) as-rolled material, b) post-rolling tempered and T6 treated material and c) T6 treated material. The macrographs illustrate the trends observed in the bending curves. The as-rolled composite laminate (**Figure 8a**) shows several delaminations between blocks, which are generally constituted by two layers. On the other hand, the post-rolling tempered and T6 treated composite laminate (**Figure 8b**) presents as many delaminations as number of interfaces. Both samples show extensive plastic deformation of the aluminum layers after the successive delaminations providing excellent toughness to the laminate. Finally, **Fig. 8c** shows a T6 treated composite laminate without post-rolling tempering in which fracture occurs by failure of brittle interfaces.

In order to obtain a better insight of the mechanism responsible of the successful delaminations of the post-rolling tempered and T6 treated sample, an interrupted bend test was also carried out. The test was stopped after the first small load drop in the bend curve at maximum load shown in **Fig. 7**, referenced as (1). **Figure 9** shows the curve of this interrupted test and also, for comparison, that from **Fig. 7**. Both curves show the same features. The first strong load drop corresponds to the cracking of the notched layer. Deformation was left to proceed just after a small load drop is observed close to the maximum strength. This drop is associated with debonding or incipient delamination in the next interface, i.e., the "interface pre-delamination" mechanism. This debonding (or pre-delamination) is not the result of crack propagation in the previous layer. It is the result of differences in mechanical behavior between the interface and the adjacent layers. Interfaces should be more brittle than the layers in order for interface pre-delamination to occur. Macrograph given in **Fig. 10** shows the delamination in the interface next to the notch for the interrupted bend tested sample. However, the debonding in the next inner interface due to the "interface pre-delamination" mechanism is difficult to observe, since no spaces are left between the layers once the load is retired.

3.2.3. Shear tests

To precisely characterize the mechanical properties of interfaces, which are responsible of the fracture behavior observed during the bend test, shear tests have been performed. **Figure 11** shows shear tests on the interfaces for the post-rolling tempered and T6 treated ADL11 composite laminate and also for the T6 treated composite laminate without post-rolling tempering. Shear stress versus shear plastic deformation has been represented. The numbers of the tested interfaces correspond to their position respect to the surface layer. For comparison, shear curves for the as-received monolithic Al 7075 and Al 2024 are included. The Al 7075 alloy shows τ= 261 MPa and γ_{max}=0.6 and the Al 2024 alloy shows τ=236 MPa and γ_{max}=1.2. In general, all interfaces of the composite laminates present lower strength and ductility than those of the monolithic aluminum alloys. The interfaces corresponding to the post-rolling tempered and T6 treated ADL11 composite laminate present higher shear strength (110-140 MPa) than those of the T6 treated ADL11 composite laminate without post-rolling tempering, which additionally shows more scattered results (between 50 and 160 MPa). Particularly, the interfaces corresponding to the ADL11 composite laminate without post-rolling tempering present lower ductility and shear strength and thus, lower interface toughness.

3.2.4. Charpy test

Charpy impact tests at room temperature were carried out and the results are reported in **Table 3.** The T6 treated ADL11 composite laminate without post-rolling tempering was not tested due its low structural integrity observed by three-point bending tests. The as-received monolithic alloys and the post-rolling tempered and T6 treated ADL11 composite laminate were tested in the crack arrester and crack divider orientations. The Charpy V-notched (CVN) energy average values for the monolithic materials in the crack arrester orientation is about 40% higher than in the crack divider orientation. The impact value for the post-rolling tempered and T6 treated ADL11 composite laminate in the crack divider orientation is 97 kJ/m^2, which is 20% higher than the calculated value with the rule of mixtures (85 kJ/m^2). In contrast, the post-rolling tempered and T6 treated ADL11 composite laminate in the crack arrester orientation, which is the most favorable condition, and that of technological importance, shows an outstanding impact energy average value (1345 kJ/m^2), which is at least twenty-one times higher than for the monolithic Al 7075 alloy and seven times higher than for the monolithic Al 2024 alloy. This high energy value in the processed composite laminate is attributed to the interface toughness obtained both by the roll-bonding processing and the consecutive thermal treatments (post-rolling tempering and T6 treatment).

Figure 12 shows the fractured Charpy tested samples corresponding to the as-received 2024 and 7075 alloys, **Fig 12a** and **12b** respectively**,** and post-rolling tempered and T6 treated ADL11 composite laminate (**Fig 12c**) in the crack arrester orientation. The as-received materials show the typical fracture behavior of monolithic aluminum materials. While in the as-received Al 2024 alloy the crack follows a defined plane the as-received Al 7075 alloy presents a heterogeneously fractured surface with a deflected crack path which can be due to its rolled microstructure having elongated grains as observed by SEM (**Figure 3a**). On the other hand, **Fig 12c** shows the excellent behavior of the post-rolling tempered and T6 treated composite

laminate, showing as many delaminations as number of interfaces. This behavior is similar to that observed in the bend test, at much lower strain rate, indicating that the same fracture mechanism is operating.

4. Discussion

In the present work, a multilayer composite laminate based on Al 7075 alloy and Al 2024 alloy has been processed delivering outstanding impact toughness. This material has been achieved by several cycles of hot rolling at 465ºC. A post-rolling tempering at 175ºC for 6h prior to T6 treatment was performed to allow recovery of the deformed microstructure.

4.1. Microstructure

The laminate constituent materials have refined their microstructure as a consequence of the hot rolling process. In general, their grain size diminished from about 10 μm to 2-3 μm, except for the grains that are close to the interface for the T6 treated composite laminate without post-rolling tempering. A comparison of the microstructures of the T6 composite laminate with and without post-rolling tempering, **Fig. 4**, reveals a finer and more homogeneous grain size throughout the post-rolling tempered sample.

The highest difference between the microstructure of the composite laminate with or without post-rolling tempering is found close to the interface. The composite laminate without post-rolling tempering shows in this region a heterogeneous grain size with not well defined boundaries (**Fig. 4c**), generally associated to partially recrystallized alloys, resulting in abnormal grain growth.

Therefore, the post-rolling tempering prior to the T6 treatment can help reducing stresses by recovery, removing dislocations and stabilizing a fine microstructure, thus reducing the driving force for recrystallization during the T6 treatment. In contrast, the T6 treatment without previous post-rolling tempering induces partial recrystallization of the most deformed regions, i.e., the regions with higher dislocation density, thus increasing grain size especially around the interfaces.

On the other hand, the microanalysis close to the interface (**Figure 5**) has shown that the extent of the Zn diffusion is not influenced by the post-rolling tempering (**Fig. 5a**); in contrast, the Cu diffusion (**Fig 5b**) is slightly higher for the post-rolling tempered sample across the interface, favoring the presence of fine grains. The higher Cu diffusion in the post-rolling tempered sample is attributed to the contribution of pipe diffusion along dislocations during the post-rolling tempering, process that can take place at intermediate temperatures. Therefore, this additional diffusion of Cu during the post-rolling tempering helps pinning (sub)grain boundaries, favoring also a finer microstructure.

4.2. Mechanical properties

Processing has an important effect upon microstructure and, therefore, upon mechanical properties, such as **microhardness**. The Vickers hardness of the post-rolling tempered and T6 treated composite laminate was higher than that for the composite laminate without post-rolling

tempering both close and far from the interface as shown in **Fig. 6**. Therefore, in this research it is assumed that the difference in microstructure, **Figs. 4a** and **4c**, and hardness between the T6 treated and post-rolling tempered and T6 treated samples can be due to recovery during the post-rolling tempering. Hence, an post-rolling tempering at a low temperature (175ºC) is sufficient for dislocation annihilation without inducing recrystallization and, thus, eliminating the driving force for recrystallization at the higher temperature of 465ºC (as required for the T6 treatment). Thus a finer microstructure of the matrix in the post-rolling tempered and T6 treated sample can lead to an increase in microhardness due to the Hall-Petch relationship.

However, grain refinement is not the main contributor to the high strength of the Al 7075 alloy [28]. According to the strengthening mechanism of age hardened aluminum alloys, an efficient distribution and a higher density of precipitates leads to a higher strength by the Orowan relationship. In this way, it is assumed that the dislocations and excess of vacancies that appeared upon quenching during the following T6 treatment will be better distributed in the post-rolling tempered and T6 treated composite laminate, which presented a more homogeneous and finer microstructure than the composite laminate without post-rolling tempering. These defects generated during the quenching increase diffusivity and favor nucleation sites for precipitates during the following precipitation hardening treatment. Therefore, a finer microstructure for the post-rolling tempered and T6 treated composite laminate will favor a more efficient precipitation hardening effect, and thus, higher microhardness.

The bend tests of V-notched Charpy samples allowed characterizing the fracture mechanisms operating during the test. The load-displacement curve corresponding to the as-rolled composite laminate, **Figure 7**, showed a low strength due to the high temperatures reached during the processing, although very high ductility. This low strength value demonstrated the necessity to carry out a T6 thermal treatment to improve the strength of the multilayer material.

It should be noted that the T6 treated composite laminate without post-rolling tempering showed high brittleness in the interface and it could not be bend tested. In contrast, the post-rolling tempered and T6 treated ADL11 composite laminate showed both high bending strength (up to 9.53 kN), and outstanding ductility, higher than the rule of mixtures. Therefore, the strength and integrity of laminate materials strongly depends on the post-rolling tempering to reduce stresses around the interfaces.

It is readily apparent from **Fig. 7** that different fracture mechanisms occur in the laminate materials respect to the monolithic ones due to the presence of the interfaces. The stepped shape of the F-d curve for the composite laminates reveals that an extrinsic fracture mechanism of delamination is operating, which enhances dramatically the laminate toughness by arresting the main crack at selected interfaces. In this way, as can be observed in **Fig. 8,** all composite laminate samples (as-rolled, T6, and post-rolling tempered and T6 treated samples) show delaminations at some interfaces (as-rolled and T6 samples) or at all interfaces (post-rolling tempered and T6 treated sample).

Additionally, an interrupted bend test for the post-rolling tempered and T6 treated composite laminate (**Fig 9 and 10**) showed a small load drop, which is associated with incipient debonding in the next interface. Thus, in this new fracture mechanism, named "interface pre-delamination", a given layer interface suffers an incipient delamination before the crack reaches that interface. The interface debonds before the main crack reaches it due to the stresses that it has to stand when the bending test proceeds. The occurrence of this interface pre-delamination mechanism while delamination in the previous interface is occurring leads to a crack bridging mechanism. Accordingly, the layer between the first delamination and the following pre-delaminated interface acts like an unbroken ligament (traditionally "crack bridging"), being necessary large amount of plastic deformation to induce a new crack in such layer. Therefore, this pre-delamination mechanism warrants delamination in every interface and thereby large amounts of plastic deformation necessary to induce a new crack in every layer by crack renucleation. The occurrence of these fracture mechanisms is responsible for the enhanced toughness of the post-rolling tempered and T6 treated ADL11 composite laminate. Previous investigations [29-31] have proposed different models to calculate the contribution of crack bridging mechanism to the toughness in ceramic/metal laminates, being the metal layer constrained between ceramic layers. In the present study, additional extrinsic fracture toughness mechanisms are present, such as delamination and crack renucleation in the ductile aluminum layers, making very difficult the calculation of each toughening mechanism separately.

Therefore, the combined treatment of post-rolling tempering at 175ºC for 6h followed by T6 treatment favors delamination of all interfaces, which is the best situation from the viewpoint of fracture mechanism to obtain outstanding impact toughness.

To characterize quantitatively the mechanical properties of the interface (strength and ductility and thus interface toughness), shear test were performed **(Figure 11).** As expected, Al 7075 is more resistant than Al 2024 but presents lower ductility and toughness. Much lower is, in average, the strength, ductility and toughness of the T6 treated composite laminate interfaces. This is in total agreement with the fact that the three point bend samples failed during testing due to premature delamination of weaker inner interfaces, as shown in **Fig. 8c**. It is our contention that quenching during the T6 treatment provokes additional stresses at the interfaces which already had a large amount of strain hardening, especially around the broken alumina particles.

On the other hand, a post-rolling tempering previous to the T6 treatment eliminates the excess of stress avoiding damage of the interfaces during later quenching. In this way interfaces can be obtained with shear strengths between 100-130 MPa (about half of the monolithics) and ductilities in average about one third that of Al 7075, which amounts to an average interface toughness of about one sixth that of Al 7075. This low interface toughness values warrant crack deflection by "interface pre-delamination" at all interfaces.

Finally, Charpy impact tests confirm the discussion regarding the bend tests. The post-rolling tempered and T6 treated ADL11 composite laminate possess higher impact energy value than the monolithic materials, more than twenty-one times than this one for the 7075-T6

aluminum alloy. Furthermore, the macrograph of the post-rolling tempered and T6 treated Charpy tested sample shows the same fracture behavior than the bend tested sample with all interfaces delaminated, which indicate that the "interface pre-delamination" mechanism operates at both high impact rate and low bending test rate.

In summary, interfaces less tough than the surrounding layers have been obtained, which warrant delamination in every interface across the composite laminate thanks to the "interface pre-delamination" mechanism. These interfaces prone to delamination were obtained by hot rolling ($\varepsilon \approx 1$) followed by a post-rolling tempering prior to the T6 treatment. This thermo-mechanical processing achieves also a very fine microstructure, excellent hardness and strength, increasing outstandingly the laminate toughness.

5. Conclusions

A multilayer composite laminate of Al 7075 and Al 2024 alloys has been developed by hot roll-bonding, resulting in a material of outstanding impact toughness. The major conclusions of the study are:

1. A post-rolling tempering at 175ºC for 6h previous to the T6 treatment was necessary to reduce stresses around the interfaces produced by the rolling process, obtaining fine microstructures and optimized precipitation hardening during the T6 treatment.

2. The post-rolling tempered and T6 treated ADL11 composite laminate showed an excellent impact energy value (1345 kJ/m^2) which is at least twenty-one times higher than for the monolithic Al 7075 alloy and seven times higher than for the monolithic Al 2024 alloy. This high impact energy of the processed composite laminate is attributed to the interfaces obtained both by the roll-bonding processing and the combined thermal treatments (post-rolling tempering and T6 treatment).

3. The mechanism of "interface pre-delamination" was responsible of delamination and crack renucleation in every layer of the composite laminate and, thus, of the excellent impact toughness obtained.

Acknowledgements

Financial support from CICYT (Project MAT2003-01172) is gratefully acknowledged. C.M. Cepeda-Jiménez and J.M. García-Infanta thank the Spanish Ministry of Education and Science for a Juan de la Cierva contract and a FPI fellowship respectively. We also thank L. del Real-Alarcón for the welding work, F.F. González-Rodríguez for assistance during hot rolling and J. Chao-Hermida for assistance with the Charpy impact test.

References

1. J.C. Williams and E.A. Starke Jr.: Acta Mater., 2003, vol. 51, pp. 5775-99.

2. J.E. Hatch (Ed.): Aluminium. Properties and Physical Metallurgy, American Society for Metals, Ohio, 1984, pp. 351-78.

3. E.A. Starke Jr. and J.T. Staley: Prog. Aerospace Sci., 1996, vol. 32 pp. 131-72.

4. T. Warner: Mater. Sci. Forum, 2006, vol.519-521, pp. 1271-78.

5. H.T. Lee and G.H. Shaue: Mater. Sci. Eng. A, 1999, vol. 268, pp. 154-64.

6. S. Ozden, R. Ekici and F. Nair: Compos. Part A, 2007, vol. 38, pp. 484-94.

7. J. Wadsworth and D.R. Lesuer: Mater. Charact., 2000, vol. 45, pp. 289-313.

8. T.M. Osman, J.J. Lewandowski and D.R. Lesuer: Mater. Sci. Eng. A, 1997, vol.229, pp. 1-9.

9. R. Alderliesten, G. Campoli and R Benedictus: Compos. Sci. Technol., 2007, vol. 67, pp. 2545-55.

10. G. Caprino, V. Lopresto and P. Iaccarino: Compos. Part. A, 2007, vol. 38, pp. 290-300.

11. T.M. Osman, P.M. Singh and J.J. Lewandowski: Scripta Metall. Mater., 1994, vol. 31, pp. 607-12.

12. H.A. Hassan, J.J. Lewandowski and M.H. Abd El-Latif: Metall. Mater. Trans. A, 2004, vol. 35, 2291-2303.

13. L.Y. Ellis and J.J. Lewandowski: Mater. Sci. Eng. A, 1994, vol. 183, pp. 59-67.

14. H.A. Hassan, J.J. Lewandowski and M.H. Abd El-Latif: Metall. Mater. Trans. A, 2004, vol. 35, pp. 45-52.

15. M. Pozuelo, F. Carreño, C.M. Cepeda-Jimenez and O.A. Ruano: Metall. Trans. A, 2008, vol.39, pp.666-71.

16. M. Pozuelo, F. Carreño and Ruano OA: Mater. Sci. Forum, 2003, vol. 426, pp. 883-88.

17. D.R. Lesuer, C.K. Syn, O.D. Sherby, J. Wadsworth, J.J. Lewandowski and W.H. Hunt Jr: Int. Mater. Rev., 1996, vol. 41(5), pp. 169-97.

18. D.W. Kum, T. Oyama, O.A. Ruano and O.D. Sherby: Metall. Trans. A, 1986, vol.17, pp. 1517-21.

19. M. Pozuelo, F. Carreño and O.A. Ruano: Compos. Sci. Technol., 2006, vol. 66, pp. 2671-76.

20. D.W. Kum, T. Oyama, J Wadsworth and O.D. Sherby: J. Mech. Phys., 1983, vol. 31, pp. 173-86.

21. H Kaçar, E Atik and C Meriç: J. Mater. Process. Tech., 2003, vol. 142, pp. 762-66.

22. N Kamikawa, N Tsuji, X Huang and N Hansen: Acta Mater., 2006, vol. 54, pp. 3055-66.

23. G.E. Dieter: Mechanical Metallurgy, SI Metric, UK, 1988, pp.12-15.

24. F. Viana, A.M.P. Pinto, H.M.C. Santos and A.B. Lopes: J. Mater. Process. Tech., 1999, vol. 92-93, pp. 54-59.

25. C. Genevois, A. Deschamps, A. Denquin and B. Doisneau-Cottignies: Acta Mater., 2005, vol. 53, pp. 2447-58.

26. C. Badini, F. Marino and E Verné: Mater. Sci. Eng. A, 1995, vol. 191, pp. 185-91.

27. L.F. Mondolfo: Aluminium alloys: structure and properties, MA.: Butterworth and Co., Boston, 1976, pp. 695-99.

28. Y.H. Zhao, X.Z. Liao, Z. Jin, R.Z. Valiev and Y.T. Zhu: Acta Mater., 2004, vol. 52, pp. 4589-99.

29. D.R. Bloyer, K.T. Venkateswara Rao and R.O. Ritchie: Mater. Sci. Eng. A, 1996, vol.216, pp.80-90.

30. D.R. Bloyer, K.T. Venkateswara Rao and R.O. Ritchie: Metall. Mater. Trans. A, 1998, vol.29, 2483-2496.

31. T.M. Osman, H. A. Hassan and J.J. Lewandowski: Metall. Mater. Trans. 39A, 2008, vol.39, 1993-2206.

Figure Captions

Figure 1. Scheme of the processing temperature of ADL11 composite laminate.

Figure 2. Scheme of the shear test.

Figure 3. SEM micrographs showing the microstructure in the LT orientation: (a) as-received 7075-T6 (D) and (b) 2024-T3 (L).

Figure 4. SEM micrographs showing internal interfaces and layers. a) interface 3 in post-rolling tempered and T6 treated ADL11 composite laminate; b) Al-7075 (D) layer in post-rolling tempered and T6 treated ADL11 composite laminate. c) interface 3 in T6 treated ADL11 composite laminate; d) Al-7075 (D) layer in T6 treated ADL11 composite laminate.

Figure 5. Atomic percentage of a) Zn composition across different interfaces and b) Cu composition across interfaces 1,2 and 5 and plotted in a single curve, as a function of the distance to the interface in ADL11 composite laminate, with and without post-rolling tempering previous to T6 treatment.

Figure 6. Microhardness Vickers (100g; 15s) of the ADL11 composite laminate with and without post-rolling tempering previous to T6 treatment as a function of the distance to the interface 5.

Figure 7. Three point bend test of as-received aluminum alloys and of as-rolled ADL11 and post-rolling tempered and T6 treated ADL11 composite laminates.

Figure 8. Macrographs of bend tests fractured samples: a) as-rolled ADL11 composite laminate; b) Post-rolling tempered and T6 treated ADL11 composite laminate; c) T6 treated ADL11 composite laminate.

Figure 9. Three-point bend test of post-rolling tempered and T6 treated ADL11 composite laminates.

Figure 10. Macrograph of post-rolling tempered and T6 treated ADL11 composite laminates showing the first delamination during the bend test.

Figure 11. Shear tests conducted on as-received aluminum alloys and different interfaces of the ADL11 composite laminates with and without post-rolling tempering previous to the T6 treatment.

Figure 12. Macrographs of Charpy tested fractured samples of (a) as-received 2024 Al, (b) 7075 Al and (c) post-rolling tempered and T6 treated ADL11 composite laminate.

Table 1. Chemical composition of as-received aluminum alloys (atomic percent).

Alloy	**Si**	**Fe**	**Cu**	**Mn**	**Mg**	**Cr**	**Zn**	**Ti**	**Ni**
7075 "D"	0.05	0.04	0.74	0.01	2.89	0.13	3.05	0.04	------
2024 "L"	0.07	0.04	2.46	0.21	1.26	0.04	0.14	0.02	0.06

Table 2. Mechanical properties of as-received aluminum alloys. (UTS= ultimate tensile strength; YS= yield point; HV= Vickers Hardness; T6=solution treating followed by quenching and finally age hardening; T3= solution treating followed by quenching, cold working and finally natural aging.

Alloy	**UTS [(a)] (MPa)**	**YS [(a)] (MPa)**	**HV**	**Elongation [(a)] (%)**
7075-T6 "D"	545	475	188	8
2024-T3 "L"	457	333	138	16

(a) Data provided by the alloy maker from tensile tests

Table 3. Charpy V-notched (CVN) (kJ/m^2) energy of as-received and composite laminate.

Material	**CVN Energy-arrester[(a)] (kJ/m^2)**	**CVN Energy-divider[(b)] (kJ/m^2)**
7075-T6 "D"	62	43
2024-T3 "L"	178	126
ADL11 + post-rolling tempering (6h-175ºC) + T6	1345	97

[(a)] Crack arrester= the notch tip is parallel to the rolling plane and rolling direction

[(b)] Divider= the notch tip is perpendicular to the rolling plane and rolling direction

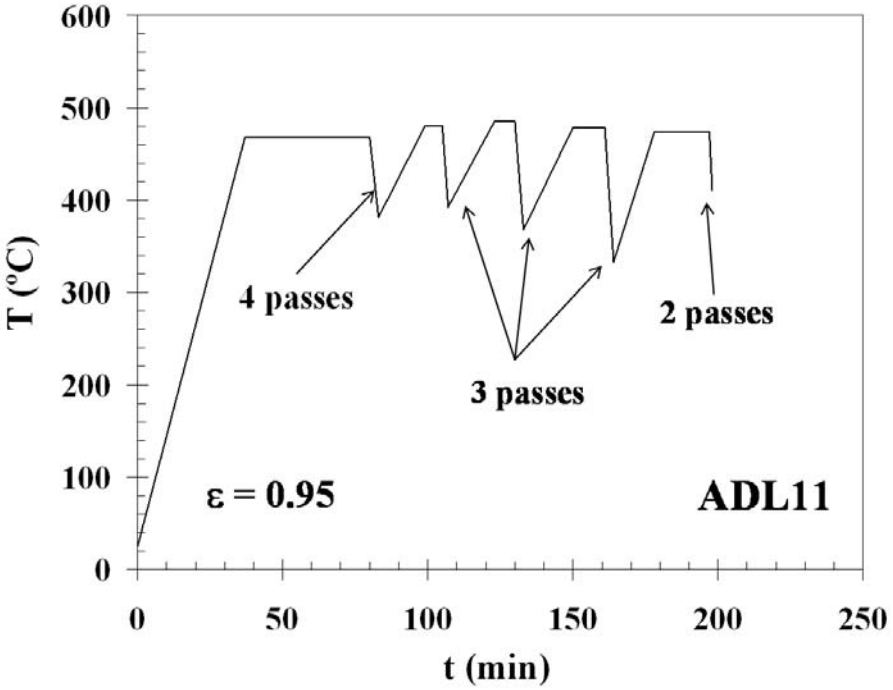

Figure 1

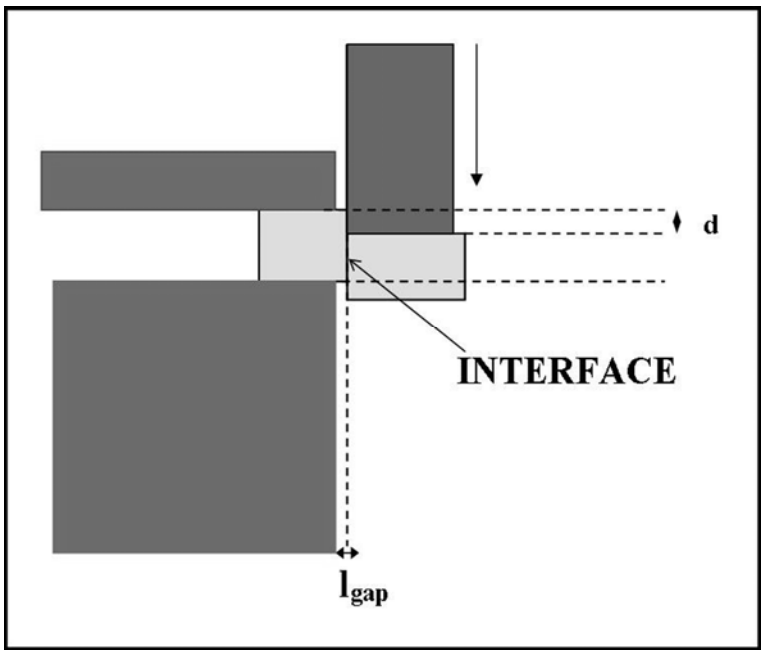

Figure 2

a) **b)**

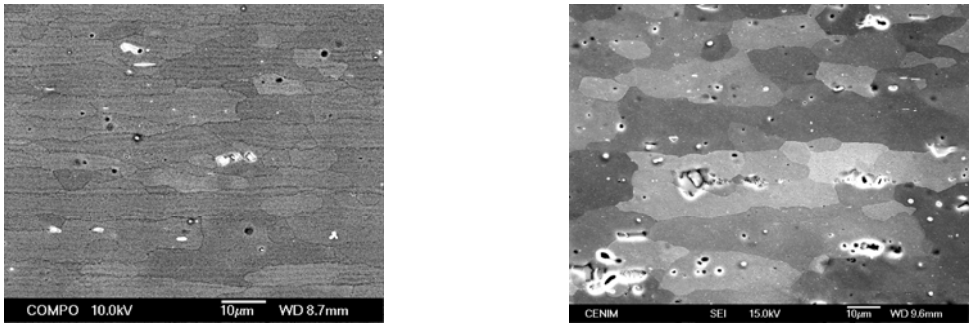

Figure 3

a) **b)**

c) **d)**

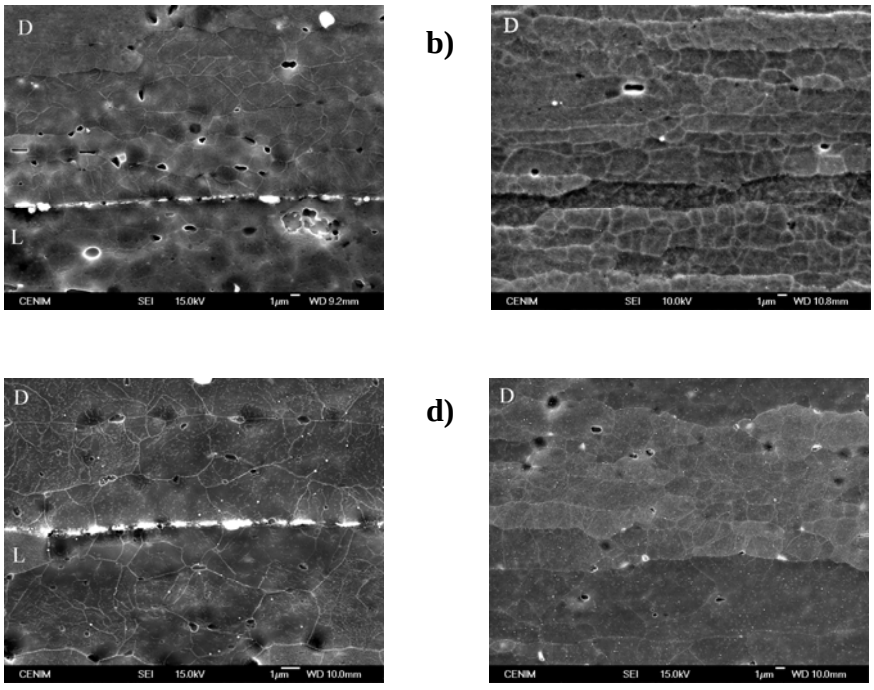

Figure 4

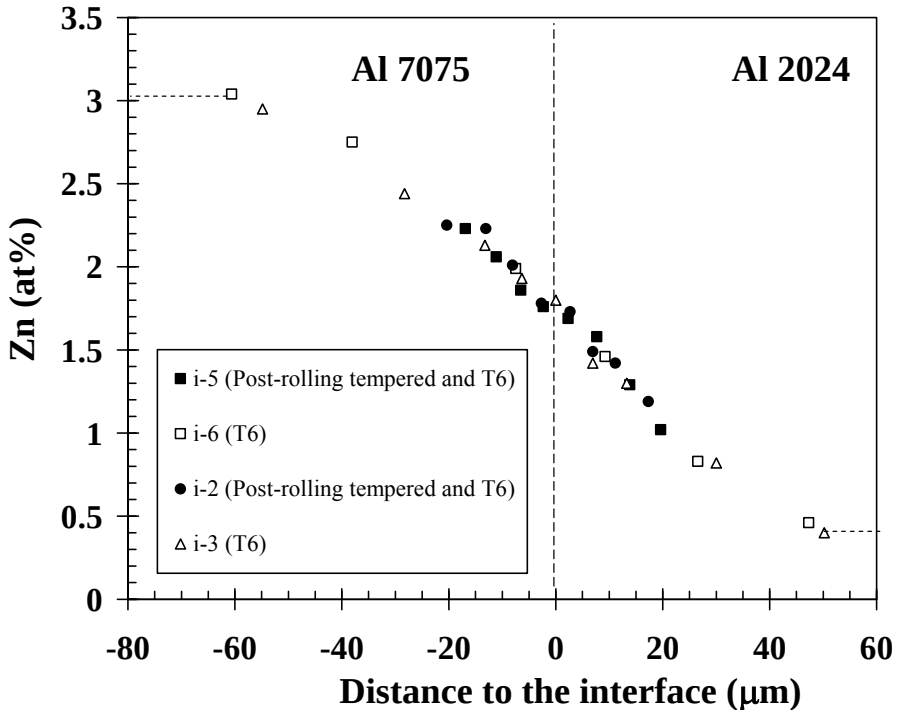

Figure 5a

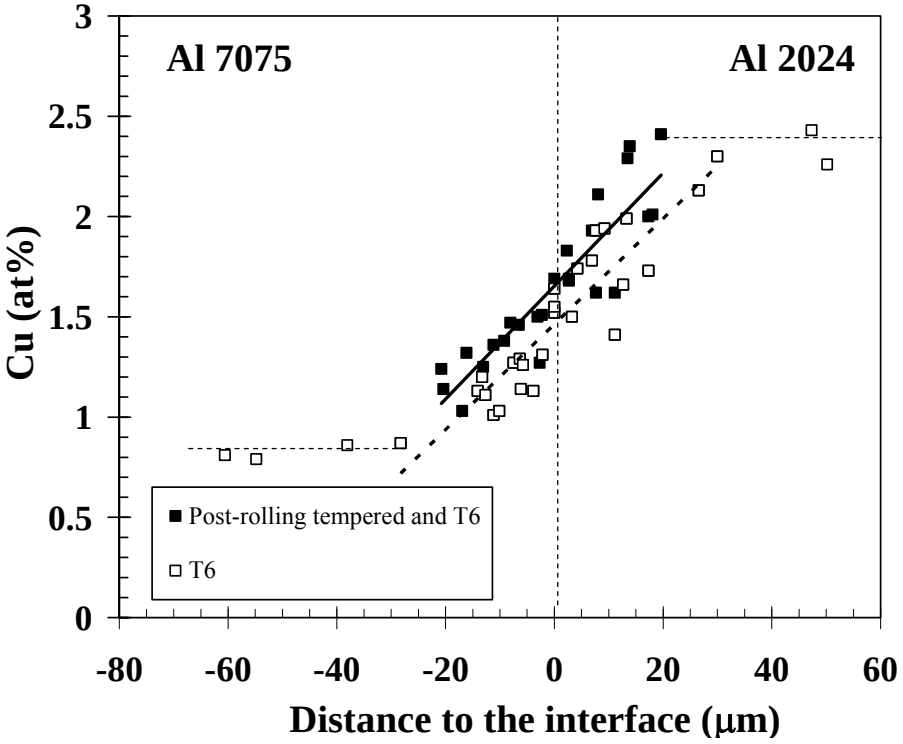

Figure 5b

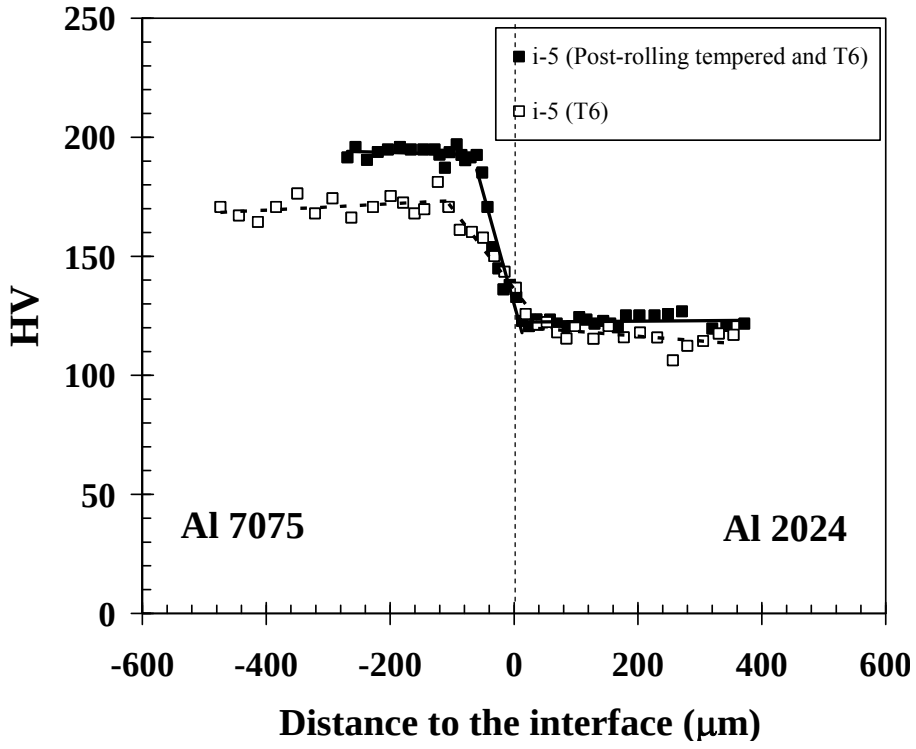

Figure 6

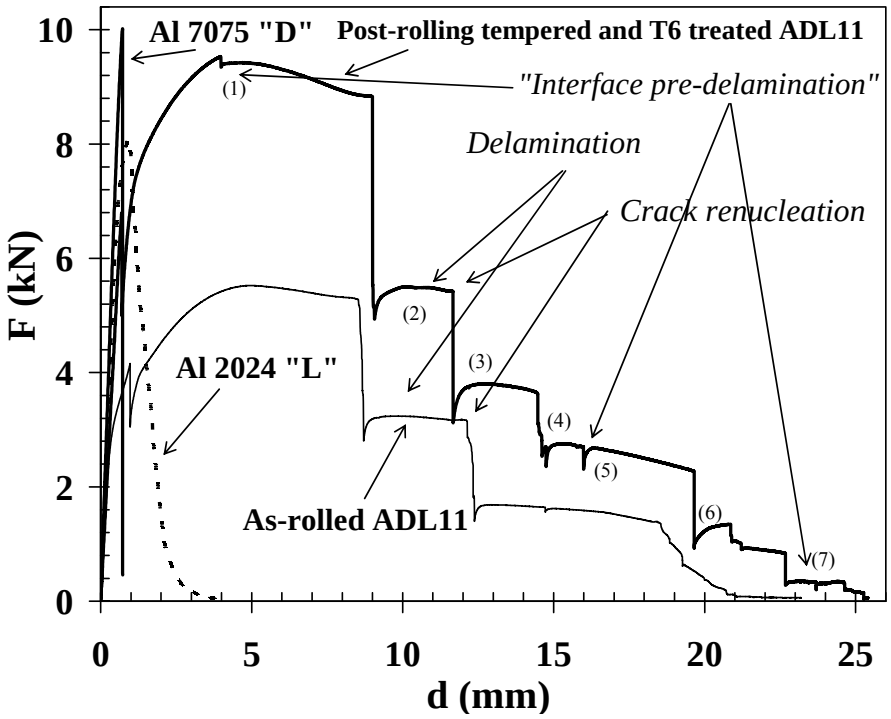

Figure 7

a)

b)

c)

Figure 8

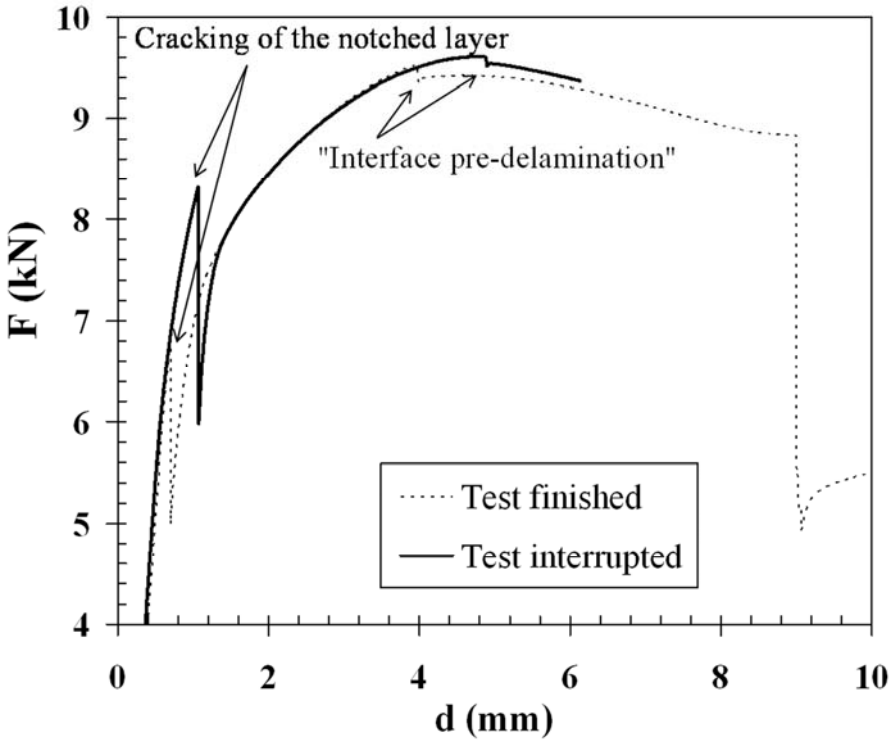

Figure 9

Figure 10

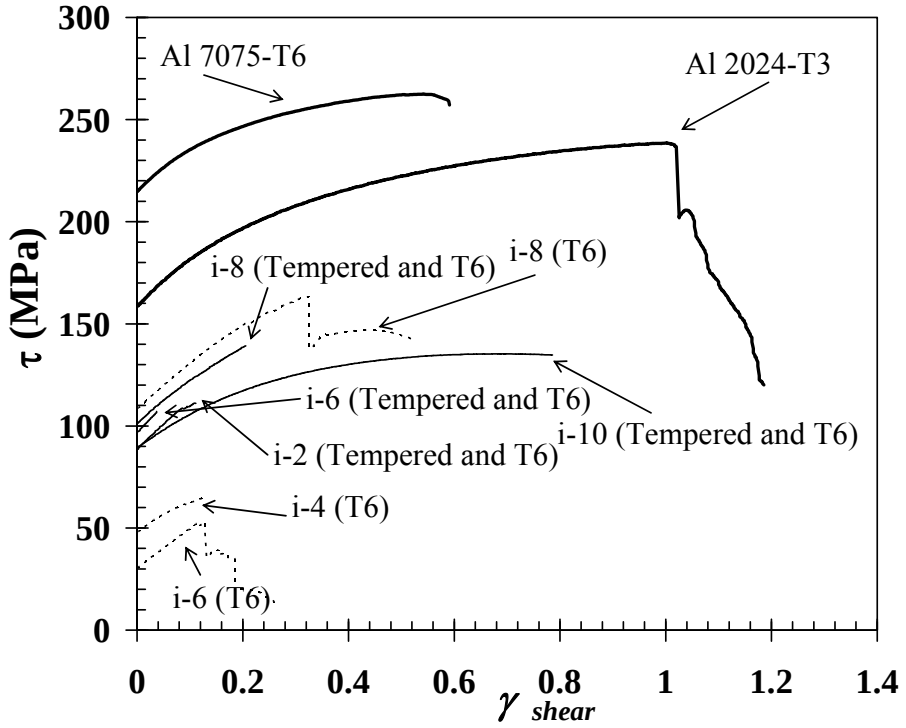
300
250
200
150
100
50
0
τ (MPa)
0
0.2
0.4
0.6
0.8
1
1.2
1.4
γ shear
Al 7075-T6
Al 2024-T3
i-8 (Tempered and T6)
i-8 (T6)
i-6 (Tempered and T6)
i-10 (Tempered and T6)
i-2 (Tempered and T6)
i-4 (T6)
i-6 (T6)

Figure 11

a)

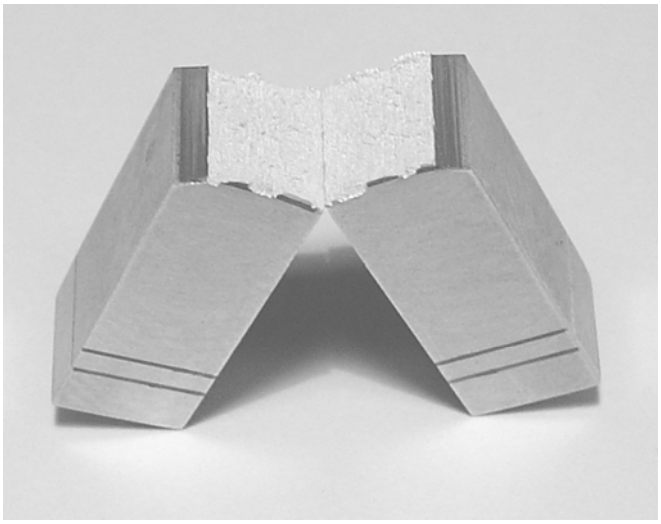

b)

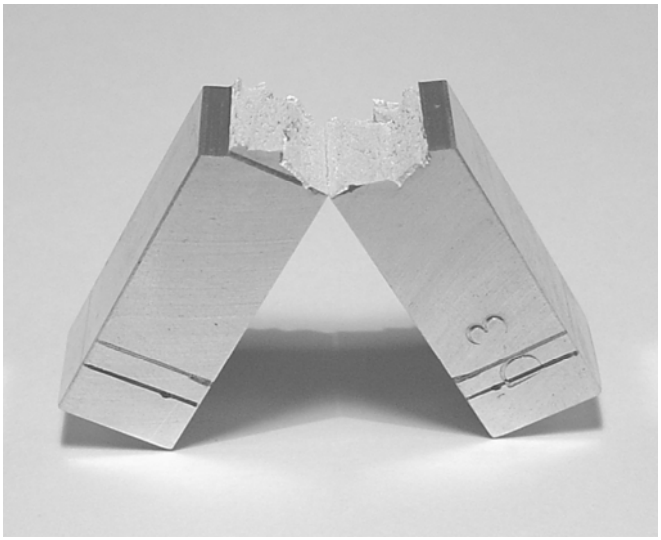

c)

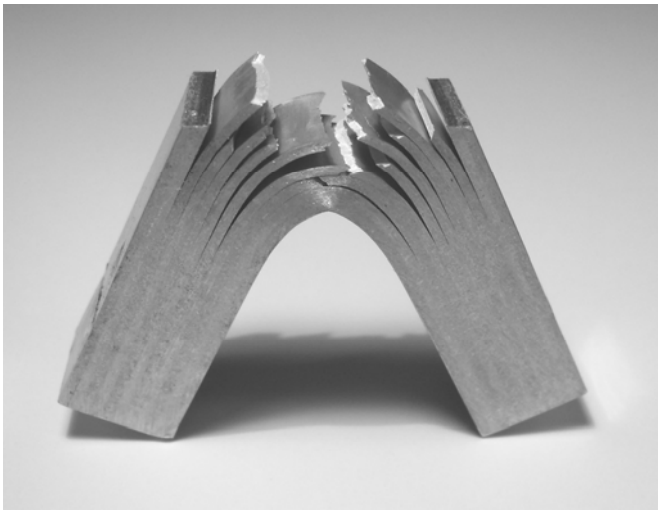

Figure 12